Li-O$_2$ Cells Based on Hierarchically Structured Porous α-MnO$_2$ Catalyst and an Imidazolium Based Ionic Liquid Electrolyte

Juqin Zeng, Jijeesh Ravi Nair [*] *, Carlotta Francia, Silvia Bodoardo, Nerino Penazzi*

Department of Applied Science and Technology - DISAT, Politecnico di Torino, Corso Duca degli Abruzzi 24, 10129 Turin, Italy.
[*]E-mail: jijeesh.nair@polito.it

Highly crystalline α-MnO$_2$ is synthesized by facile reduction of KMnO$_4$ in acidic solution. The obtained α-MnO$_2$ exhibits high specific surface area of about 156 m^{2}g^{-1} with a hierarchical bimodal porous structure. It is a promising electro-active material that can act as an oxygen reduction catalyst to improve the recharge ability of lithium-oxygen cells. TEM analysis confirmed that α-MnO$_2$ is highly crystalline and exists in the form of nano-rods forming spherical aggregates. The cell with α-MnO$_2$ as catalyst and commercially available imidazolium-based room temperature ionic liquid with LiClO$_4$ as electrolyte displayed an initial discharge capacity of 900 mAhg^{-1} which, after prolonged cycling, reached a stable value of about 600 mAhg^{-1} with high recharge efficiency (∼ 90%) and good capacity retention. Thus, α-MnO$_2$ catalyst along with ionic liquid based electrolyte can be an effective combination to obtain improved capacity and durability in rechargeable lithium-O$_2$ batteries.

1. INTRODUCTION

Even though continuous improvements have been achieved, Li-ion batteries are near to its theoretical limit of energy density and further increase in performance would be a real challenge [1]. Rechargeable Li-O$_2$ batteries have the potential to provide at least 5 times the gravimetric energy density than the conventional Li-ion batteries if the problems related to their commercial application are properly addressed [2]. High practical specific energy values of 500–900 Whkg^{-1} have been reported for a Li-O$_2$ battery [3], and such values are attractive especially for automotive applications where a significant increase in specific energy will be required to achieve a driving range more than 550 km [4]. Moreover, at present, each components of the cell has serious long term performance issues which needs to be addressed to ensure the development of an appropriate system.

The basics of non-aqueous rechargeable Li-O_2 cell resides in the reversible formation and decomposition of lithium peroxide (Li_2O_2) at the cathode during the discharge and the recharge processes respectively. One of the key points is the lowering of the Li_2O_2 oxidation over potential at the cathode. In general, it is believed that electro-catalysts play a vital role in improving the cycling capability of Li-O_2 cells [5,6]. Generally the electro-catalyst in the cathode of Li-O_2 cell would significantly contribute to oxygen reduction reaction (ORR) and oxygen evolution reaction (OER), and serious efforts have been made to develop electro-catalysts for rechargeable Li-O_2 cells [7-9]. Several Authors have proposed the role of catalysts to reduce the voltage gap between the discharge and recharge processes and thus increasing the round efficiency of the cells [10,11]. The cycling ability and the capacity of the cells are generally related to the nature of electro-catalyst at the cathode. Among various catalysts explored for the Li-O_2 cell, the MnO_2-based catalysts, including MnO_2 with different structures, MnO_2 combined with noble metals [12] and MnO_2 supported on carbons [13], are of particular interest due to their low cost, low toxicity and good structural stability.

Cheng et al. [14] compared some metal and metal oxide catalysts (Pd, Pt, Ru, PdO, RuO_2 and MnO_2) under charge/discharge conditions and confirmed that the Li–O_2 batteries with MnO_2 catalyzed cathodes showed higher discharge capacities and cycle ability when compared to other counterparts. Li-O_2 cells with α-MnO_2 nanowires catalyzed cathodes showed very high charge storage capacity and excellent capacity retention by avoiding deep discharge [15]. Li et al. [16] reported mesoporous α-MnO_2 hollow urchins with high BET surface area of 132 m^2g^{-1} which showed a high capacity in the first charge/discharge process as well as a good cycling performance. Zhang et al.[17] discovered that the discharge capacity and cycling ability of the Li-O_2 cells increased significantly with the air electrode made of α-MnO_2 catalyst due to the reaction between the discharge product Li_2O_2 and α-MnO_2 during charging reactions. Thapa et al. [12] prepared a Pd/mesoporous α-MnO_2 electrode which is highly active as Li-O_2 battery air electrode and displayed high energy efficiency during charge/discharge.

However, some recent investigations showed that side reactions with organic carbonate based electrolytes are more severe and provide a rationale for the compromised reversibility in such systems. [10,18]. Recent studies enlightened the real catalytic action of α-MnO_2 nanowires towards the decomposition of hydrogen peroxide and a strong correlation between the rate of H_2O_2 decomposition and the charging voltage of the Li–O_2 cell was observed [19]. Mesoporous α-MnO_2 nano-sphere structures also demonstrated [20] good electro-catalytic properties for the reduction of H_2O_2 in alkaline medium. Thus, organic carbonates-based electrolytes, so commonly used in lithium ion batteries, are unsuitable electrolyte solvents for Li-O_2 cells [21]. In fact, the Li-O_2 chemistry is just characterized by an apparent reversibility and the observed cell cycling has been mostly attributed to the consumption of the carbonate solvents during discharge and decomposition of lithium alkyl carbonates during re-charge [21,22].

Recently, Jung H-G. et al. [23] proposed an optimized glyme-based electrolyte, able to stand for many cycles at high current rates without any decay in capacity. Although ether-based electrolytes should possess higher stability with respect to organic carbonates in the Li–O_2 cell, mass spectrometry measurements pointed out that only 60% of the O_2 consumed during discharge was released during re-charge, when a dimethoxyethane–based electrolyte was employed [24]. Extremely high capacity

retention and good cycle life (up to 100 cycles) were achieved with a $Li-O_2$ battery based on dimethyl sulfoxide electrolyte [25].

Thus, properties such as electrolyte stability, along with other basic electrolyte properties as high Li^+ conductivity, viscosity, polarity, high O_2 solubility and diffusion, low volatility to avoid evaporation at the cathode, account for basic requirements to ensure the proper overall operation of $Li-O_2$ cells. Nevertheless, room temperature ionic liquids (RTILs), largely employed in lithium ion batteries [26,27] have also been proposed as suitable electrolyte for $Li-O_2$ cells [23,25] due to their high conductivity, non-volatility, non-flammability and wide temperature range of operations. It has been reported that RTILs exert a beneficial action on the kinetics at the cathode of a Li-air cell and this behaviour was attributed to the build-up of a less resistive film at the cathode/air/electrolyte interface as well as to improve Li_2O_2 solubility in the RTIL, leading to a reduced Li_2O_2 particles size[28]. Kuboki et al. [29] examined the hydrophobicity of some RTIL in the lithium-air cell and considered EMITFSI (1-ethyl-3-methylimidazolium bis(trifluoromethylsulfonyl)amide) as a suitable electrolyte component due to their capability to prevent the vaporization of electrolyte and hydrolysis of anode. The ORR was investigated on gold electrodes in EMITFSI by cyclic voltammetry and a high rechargeable ORR was observed together with Li_2O and Li_2O_2 formation [30].

Relying on these considerations we developed a highly crystalline $\alpha-MnO_2$ for a $Li–O_2$ cell, with high specific surface area and a hierarchical bimodal porous structure. This material possess some interesting features that can be exploited to improve the performances of the cathode in a $Li–O_2$ cell. The cathodes were tested in $Li-O_2$ cells containing pure RTIL (solvent) and $LiClO_4$ salt, thus the complete absence of carbonates were ensured. As we mentioned before, several critical factors influence the sustainable recharge-ability of $Li-O_2$ cells and it is difficult to analyze all the causes affecting their degradation in one shot. The energy storage capability of $Li-O_2$ cells are strongly determined by the oxygen electrode which mostly contributes to the voltage drop of the system [31,32]. However, when the oxygen electrode consists of porous materials capable to reach such high storage capacities, the other components may become one of the vital factors which limits the performance of the cell.

Keeping in mind all the above mentioned points we have investigated a possible combination that could act as a suitable electrolyte (EMITFSI + $LiClO_4$) along with a highly porous $\alpha-MnO_2$ cathode catalyst. This combination can allow the built up of an efficient $Li-O_2$ cell with high capacity ($900 \ mAhg_{MnO2+C}^{-1}$) and excellent capacity retention. The highly crystalline $\alpha-MnO_2$, prepared through a very easy synthesis, showed excellent catalytic activity in lowering the Li_2O_2 oxidation over potential and excellent stability upon cycling.

2. EXPERIMENTAL

Unless and until mentioned separately, the chemicals used in the study are analytical grade and used as received from Sigma Aldrich.

2.1 α-MnO₂ preparation and characterisation

The α-MnO$_2$ precursor solution was prepared by modifying the procedure reported in ref. [12]. In a typical procedure, 3 g of potassium permanganate (KMnO$_4$) and 10 ml of H$_2$SO$_4$ (98 wt.%, 2 M) were added in to 90 ml of de-ionised water under magnetic stirring to form the precursor solution. This precursor was heated at 80 °C for 6 h under constant stirring. The precipitate was filtered and washed with distilled water. The final product was dried at 120 °C for 6 h under high vacuum.

The morphology of the samples was examined using field-emission scanning electron microscopy (FESEM, JEOL-JSM-6700F). Nitrogen adsorption isotherms at 77 K were recorded by a Micromeritics ASAP-2010 Instrument. The XRD patterns were collected with a Philips X-Pert MPD X-ray diffractometer equipped with a CuKα radiation. TEM was performed by the Philips CM12. X-ray photoelectron spectroscopy (XPS) measurements were carried out with a Physical Electronics PHI 5800 (USA) multi-technique ESCA system using monochromatic Al-Kα X-ray radiation with a beam size of about 400 × 400 μm.

2.2 Electrolyte preparation and characterisation

The organic electrolyte, 1.0 M lithium perchlorate (LiClO$_4$) in 1:1 wt/wt ethylene carbonate (EC)-diethyl carbonate (DEC), was used as standard electrolyte. The RTIL based electrolyte was prepared by dissolving LiClO$_4$ (5 wt.%) in RTIL 1-ethyl-3-methylimidazolium bis(trifluoromethylsulfonyl)imide (EMITFSI). LiClO$_4$ was selected due to its proven chemical stability in the presence of Li$_2$O$_2$ [33].

The ionic conductivity [34] of the EMITFSI-LiClO$_4$ was determined by electrochemical impedance spectroscopy (EIS) analysis of cells formed by using separators (glass wool separator, whatman GF/A) of area 0.785 cm^2 between two stainless-steel 316 (SS-316) blocking electrodes. A PARSTAT-2273 potentiostat/ galvanostat/F.R.A. (Frequency Response Analyser) instrument (Princeton Applied Research, USA) was employed for measurements at various temperatures ranging from 20 °C to 80 °C, over a frequency range of 1 Hz to 100 kHz at the open circuit voltage (O.C.V.). The electrochemical stability window (ESW) of the electrolytes was evaluated at ambient temperature by linear sweep voltammetry (LSV) in 3-electrodes configuration with Polypropylene-made T-cells (active area equal to 0.785 cm^2) using an Arbin Instrument Testing System model BT-2000. Separate LSV tests were carried out on each electrolyte samples to determine the cathodic and anodic stability limits. The measurements were performed by scanning the cell voltage from the O.C.V. towards more negative (cathodic limit) or positive (anodic limit) voltages. Cell configuration adopted for anodic scan (potential scan range from O.C.V. to 5.5 V vs. Li/Li$^+$): acetylene black over Al current collector as working electrode and Li metal as counter and reference electrodes using the whatman-GF/A soaked in EMITFSI-LiClO$_4$ as electrolyte; cathodic scan (from O.C.V. to -0.2 V vs. Li/Li$^+$): Cu foil as working electrode and Li metal as counter and reference electrodes using the whatman-GF/A soaked in EMITFSI-LiClO$_4$ as electrolyte. In both cases, the potential was scanned at the rate of 0.100 mV s^{-1}. The current onset of the cell was associated with the decomposition voltage of the electrolyte.

2.3 Air cathode preparation

The air cathode was prepared as a thin film over carbon paper GDL (SIGRACET GDL-24BC, SGL Technologies) based current collector. A N-methyl-2-pyrrolidone (NMP) slurry of previously prepared α-MnO$_2$ was mixed with acetylene black (Shawinigan Black AB50, Chevron Corp., USA) as electronic conductor and poly-(vinylidenefluoride) (PVdF, Solvay Solef-6020) as binder in the weight ratio of 50:35:15 respectively, was deposited over GDL using doctor blade technique. This film was dried at 55 °C overnight to obtain a composite cathode with an electrode mass of about 1.8 mgcm^{-2}. An O$_2$ electrode composed of AB50 (85 wt.%) and PVdF (15 wt.%) was also tested for comparison. A dual pore oxygen cathode was prepared thus it was composed of two interconnected porosity systems: a catalysed and a non catalysed side. The non-catalyzed system (carbon paper GDL with a micro-porous layer) can allow the transport of oxygen into the electrode even when the catalyzed system becomes eventually blocked by reaction precipitates [35].

2.4 Li-O$_2$ Cell assembly and testing

The Li-oxygen cell was then assembled in an Ar-filled dry glove box (Mbraun Labstar) using an ECC-Air electrochemical cell (EL-Cell, GmbH) configuration with openings allowing oxygen to enter the cathodic part. A lithium disc (Chemetall s.r.l.) was used as the anode and whatman-GF/A was used as the separator. The separator was saturated with the LiClO$_4$-based electrolyte either with organic carbonate or EMITFSI as solvent. The disks of oxygen electrode had an area of 2.54 cm^2. The cells were galvano-statically cycled by an Arbin BT-2000 battery tester at room temperature between 4.25-2.15 V vs. Li$^+$/Li at a current density of 0.1 mAcm^{-2}. During the tests, pure O$_2$ was continuously circulated at the O$_2$-cathode (flow rate of 8 ml min^{-1}).

3. RESULTS AND DISCUSSIONS

3.1 Structural characterization

The XRD pattern of the prepared α-MnO$_2$ is given in Fig. 1a. The X ray diffraction peaks are clearly indexed to the pure tetragonal phase of α-MnO$_2$ (JCPDS 44-0141), with lattice constants of a = 9.78 Å and c = 2.86 Å [36]. No peaks were observed for other types of crystals or amorphous MnO$_2$ which confirmed the purity of the prepared sample.

The pore structure of α-MnO$_2$ was investigated by N$_2$ sorption technique at 77 K. The resulting isotherm is shown in Fig. 1b along with the BJH (Barrett-Joyner-Halenda) pore size distribution (inset), clearly indicating a hierarchical pore structure. The isotherm curve showed two substantial hysteresis loops which clearly indicated the bimodal porous nature of the prepared MnO$_2$. The clear hysteresis loop at high relative pressure (e.g., $P/P_0 > 0.8$) was the indication of the existence of additional inter-particle mesoporous structure [37]. The Brunauer-Emmett-Teller (BET) specific surface area (SSA) of the sample was calculated from N$_2$ adsorption and the obtained values were as high as 156.9 m^{2}g^{-1}. The high SSA and the hierarchical bimodal pore structure should provide the

possibility of an efficient mass transport in the air electrode and consequent performance enhancement in the final cell.
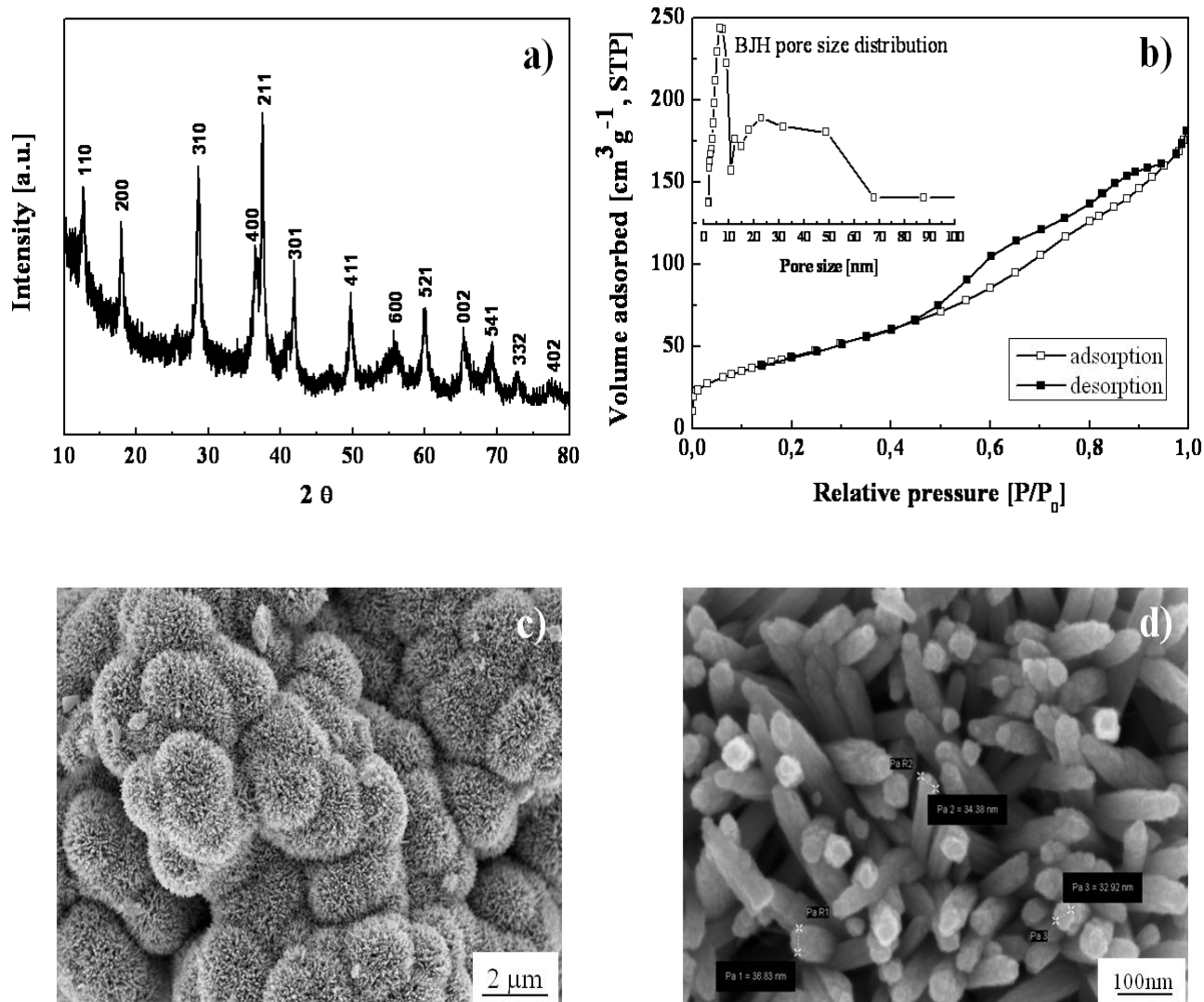
Figure 1. Characteristics of synthesized α-MnO$_2$: a) XRD pattern; b) N$_2$ sorption isotherm and BJH pore size distribution (inset); c) FESEM micrograph at 25000 magnification and d) at 400,000 magnification.

The morphology of α-MnO$_2$ was investigated by FESEM; the corresponding micrographs are shown in Fig. 1(c and d). The sphere-like micro-particles with an average diameter of ~2 μm were aggregated each other, are clearly visible in Fig. 1c. At higher magnification (Fig. 1d), the particles appeared to be solid urchins, homogeneously composed of densely aligned nano-rods. The nano-rods displayed uniform diameter of ~ 34 nm and average length of ~200 nm.
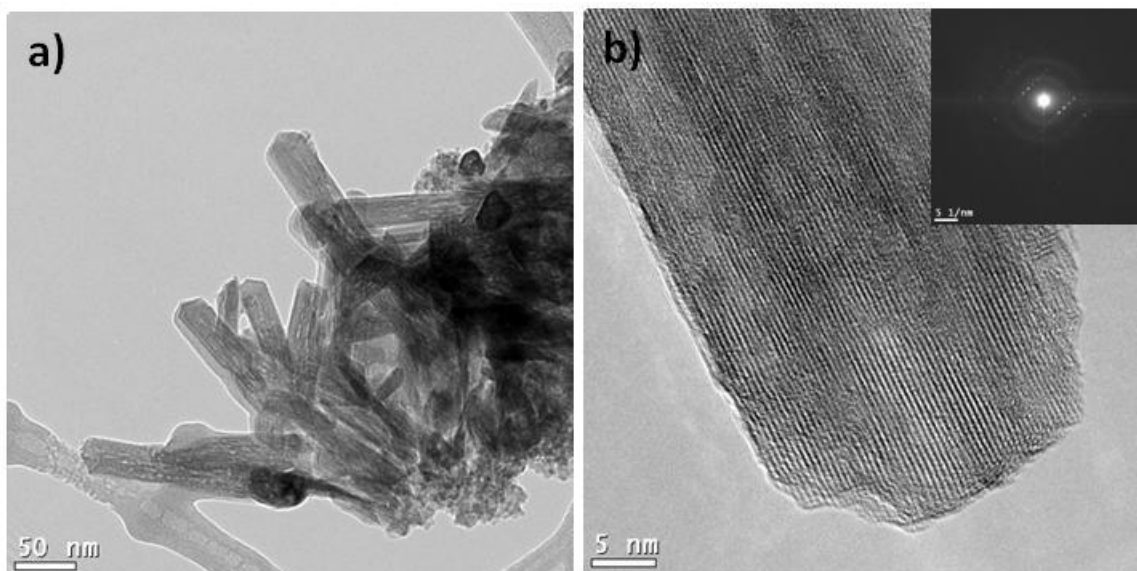
Figure 2. TEM images of synthesized α-MnO$_2$: a) α-MnO$_2$ crystals with average dimension of 30x200nm. b) single nano-rod of α-MnO$_2$; the inset shows the SAED pattern obtained by focusing on the single nano-rod.

Figure 2 shows the TEM images of the synthesised α-MnO$_2$. An average crystal dimension of 30x200nm for the nano-rods is verified in Fig. 2a. A single nano-rod is shown in Fig. 2b which clearly indicates a smooth surface. The SAED pattern (inset of Fig. 2b) based on a single nano-rod confirms the single-crystalline nature of the α-MnO$_2$ with an inter-plane distance of 6.9 Å.

XPS was employed to analyse the composition and oxidation states of the synthesized MnO$_2$. The XPS spectra are referred to a C 1s value of 284.6 eV.
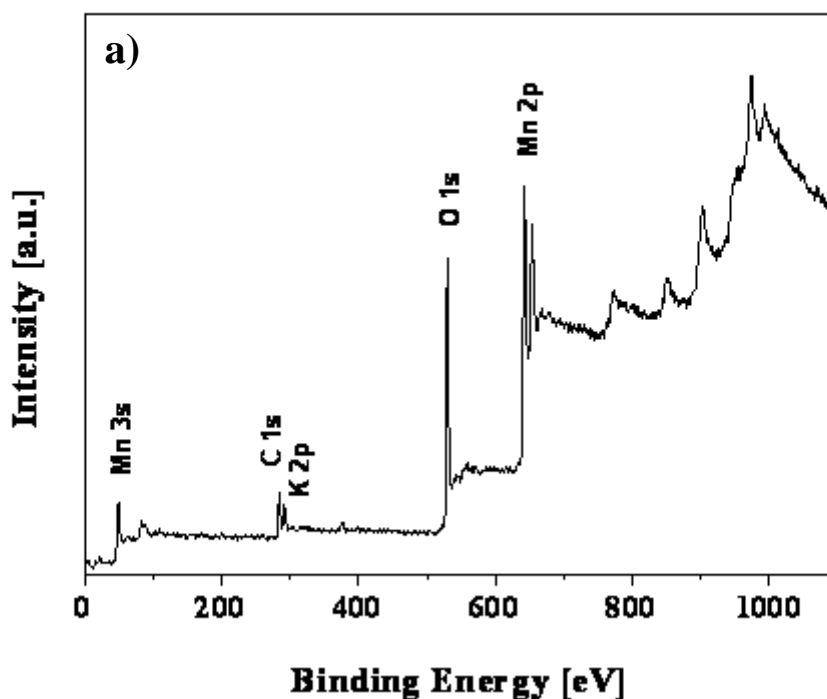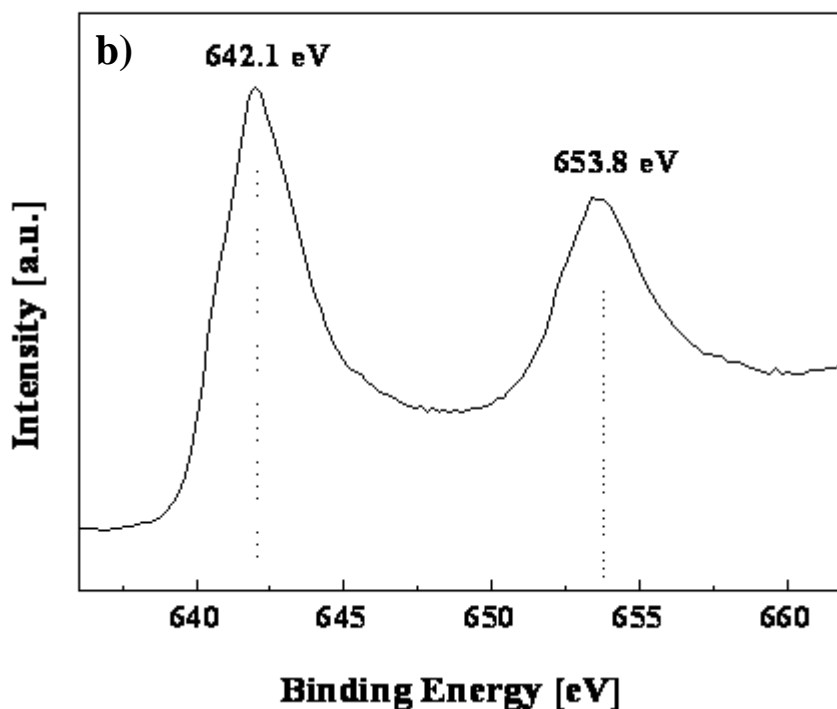
Figure 3. a) XPS survey spectrum; b) XPS high-resolution spectrum of the Mn 2p region of the obtained material

As shown in (Fig. 3a), the wide survey profile of the prepared material showed pronounced Mn and O peaks with a small amount of contaminants like C and K. The presence of small amount of K enables MnO_2 to offer more sites for Li^+ accommodation, facilitating the potential application for electrode materials in Li-based batteries [38]. The manganese oxidation state was also estimated from the high-resolution spectrum of the Mn 2p region (Fig. 3b). The XPS spectra were almost symmetrical, with Mn 2p 3/2 and Mn 2p 1/2 located at 642.1 eV and 653.8 eV, respectively, indicating a single component corresponding to binding energies of Mn(IV)-O [39,40].

The overall morphological characterisation by FESEM, TEM, XRD, N_2 absorption and XPS analyses confirms that the synthesised α-MnO_2 has dual porous nature, it is highly crystalline, it possess a nano-rod structure aggregated in the form of clusters with the typical characteristics of a pure α-MnO_2 crystal. The characteristics also suggests that the materials could be an ideal active catalyst at the oxygen cathode for the reduction of lithium peroxide.

3.2 Electrochemical characterisation

3.2.1 Electrolyte properties

Repeated and prolonged cycling ability has been considered as one of the most challenging issues for non-aqueous Li–O_2 cells [13,41]. The role of electrolyte in this regard cannot be neglected

and it is one of the biggest obstacles that need to overcome if we have to realise a stable and rechargeable Li-air battery [42], thus selection of a proper electrolyte which is stable in oxygen-rich electrochemical condition is under intense scrutiny. The ionic conductivity of the indigenous electrolytes based on EMITFSI/LiClO$_4$ showed a conductivity $>2*10^{-3}$ Scm^{-1} at room temperature and it was increased to $>1*10^{-2}$ Scm^{-1} with an increase in temperature. To determine the stability window of the indigenous electrolyte based on EMITFSI/LiClO$_4$, a blank test was carried out to determine the current–voltage response of the cell using a plain carbon support (without oxygen flow) for oxidation stability and with Cu electrode for reduction stability. Fig 4 represents the results, demonstrating that a large current flow (indication of major and irreversible decomposition of electrolyte) occurs around 4.9 V versus lithium. On the other hand for cathodic stability test, the unwanted and irreversible reactions take place around 1.5V versus lithium. Thus the working electrochemical stability range for the indigenous electrolyte was between 1.5 V to 4.9 V vs. Li/Li$^+$. The tests were carried out on fresh samples without oxygen flow. The obtained results indicated that the prepared electrolyte can be used effectively for lithium air battery applications up to a potential of 4.9V vs. Li/Li$^+$. Moreover, the current–potential curves showed very low residual current prior to breakdown voltages, confirming the purity of the used materials and experimental conditions. The results of cathodic stability also suggest that the EMITFSI-LiClO$_4$ electrolyte is capable of transporting lithium ions and eventually plating and stripping process can occur at the counter electrode.
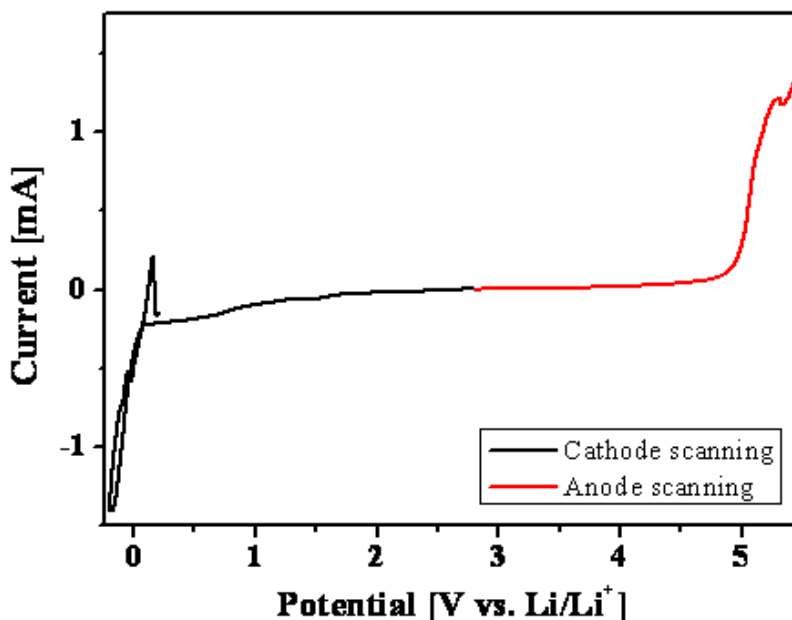
Figure 4. Electrochemical stability window of the EMITFSI-LiClO$_4$ electrolyte at 20°C. Potential scan rate: 0.100 mV s^{-1}.

3.2.2. *Catalytic activity of α-MnO$_2$*

The prepared α-MnO$_2$ was studied as an electro-active material in the O$_2$-cathode of a Li-O$_2$ cell. Before establishing the application as electro-active component it was necessary to confirm the

ORR capability at the O₂-cathodes of a Li-O₂ cell (with and without the presence of α-MnO₂). The typical lithium-O₂ cells were prepared as reported in section 2.3. The galvanostatic cycling measurements were carried out between the potential window 4.25 – 2.15 V versus Li/Li⁺, at a discharge current density of 0.1 mAcm⁻², using the electrolyte with a composition of 0.50 M LiClO₄ in pure EMITFSI-RTIL. Fig. 5 refers to the initial discharge-charge profiles for the two cells that has been prepared with and without α-MnO₂ in the oxygen cathode. The cell with α-MnO₂ showed an initial discharge capacity of 900 mAhg⁻¹ with a large and flat discharge plateau around 2.75 V vs. Li/Li⁺. The corresponding recharge capacity values were slightly lower with a voltage plateau at 3.9 V. The cell without α-MnO₂ exhibited a lower discharge capacity with a discharge plateau around 2.48 V with a specific discharge capacity of 756 mAhg⁻¹. The obtained specific capacity and nature of the profile gives good grounds to hypothesize a direct action of α-MnO₂ as electro-catalytic material, which positively enhances the discharge capacity. The α-MnO₂ oxygen electrode displayed a lower discharge/recharge voltage gap of 1.28V, with the OCV located at 3.36V. The discharge/recharge voltage gap of cathode without α-MnO₂ was slightly larger (1.29 V) with the OCV of the cell set at 2.85 V. It means, the addition of α-MnO₂ really increases the OCV (approximately 0.53V) of the cell, and an overall potential enhancement in the discharging and recharging process. The potential enhancement in the discharging process is really encouraging and it would directly enhance the specific power density of the cell.
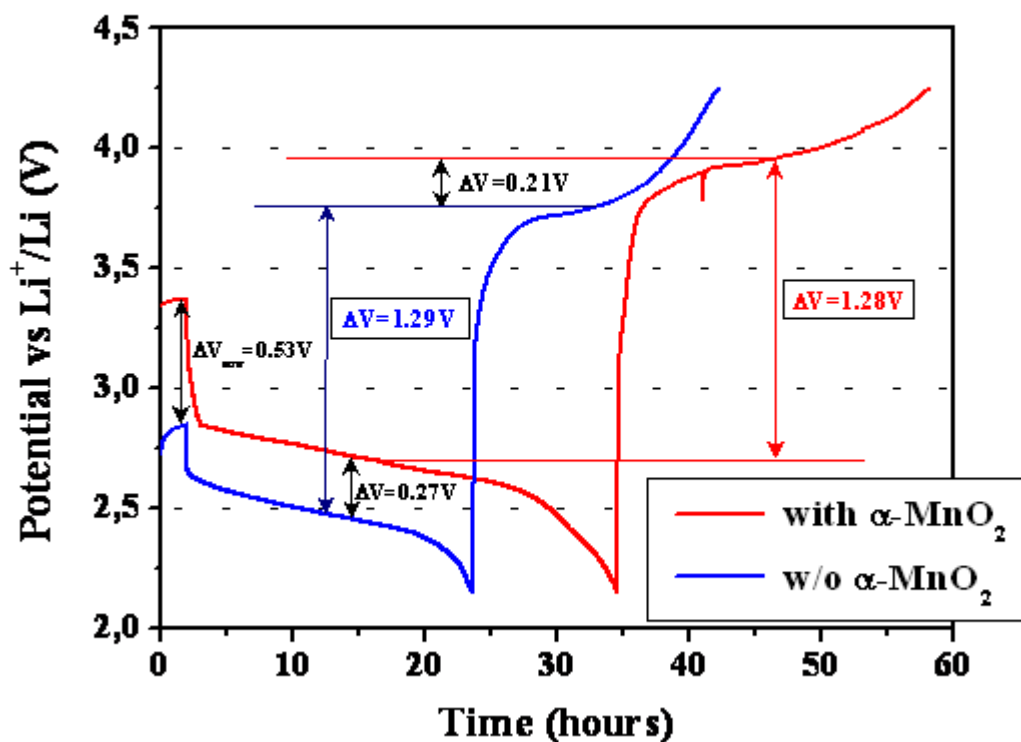
Figure 5. The first discharge/charge profiles of the Li-O₂ cells with and without α-MnO₂.

Such effects can also be considered to result from the unique crystal structure and the porosity of α-MnO₂. The crystal structure of the α-polymorph consists of 2×2 tunnels formed by edge- and

corner-sharing MnO_6 octahedral. According to the mechanism reported by Johnson [43] Li_2O_2 can be incorporated within the MnO_2 tunnels with the O_2^- ions located at the tunnel centres and the Li^+ ions coordinated between these central O_2^- ions, the latter forming the walls of the tunnels. The ability of α-MnO_2 to incorporate Li_2O_2 suggests the possibility of incorporating the Li^+ and O_2^{2-} ions on the surface of the material promoting the reversibility of the Li_2O_2 formation [15]. In our case, the over potential of oxygen evolution reaction (OER) is much higher than that of ORR, considering that the equilibrium redox potential is 2.9 V vs. Li/Li^+, which indicates that α-MnO_2 is more effective for ORR [44]. Another possible explanation of the favourable effect of α-MnO_2 is that the high surface area and the optimized pore size of α-MnO_2 which may alter the morphology of the lithium peroxide that formed during the discharge. It has also been suggested that in the presence of the catalyst, the Li_2O_2 deposits may be less dense and more porous than the one's formed in the absence of the catalyst hence preserving the ability of the reagents to diffuse into the carbon voids through the orifices occupied with such porous deposits. This may in turn increase the discharge capacity [45].

Thapa et. al. reported a similar mesoporous α-MnO_2 crystal and found that the application of Pd/mesoporous α-MnO_2, which was mixed with teflonised acetylene binder (TAB), as air electrode is effective for decreasing the charge potential and also improved the energy efficiency as well as cycling ability [12]. Nevertheless, in all the cases, the cell electrolyte was based on organic carbonates solvents, which may lead to some complicated explanations about the results obtained [46]. The initial results on the activity of α-MnO_2 encouraged us to proceed further with the cycling studies using this new combination of electrolytes.

The stabilizing effect exerted by the RTIL on the discharge-charge performances of the Li–O_2 cell is evident from Fig. 6a, where two cells containing α-MnO_2 at the cathode were tested with different kinds of electrolyte under same experimental conditions.
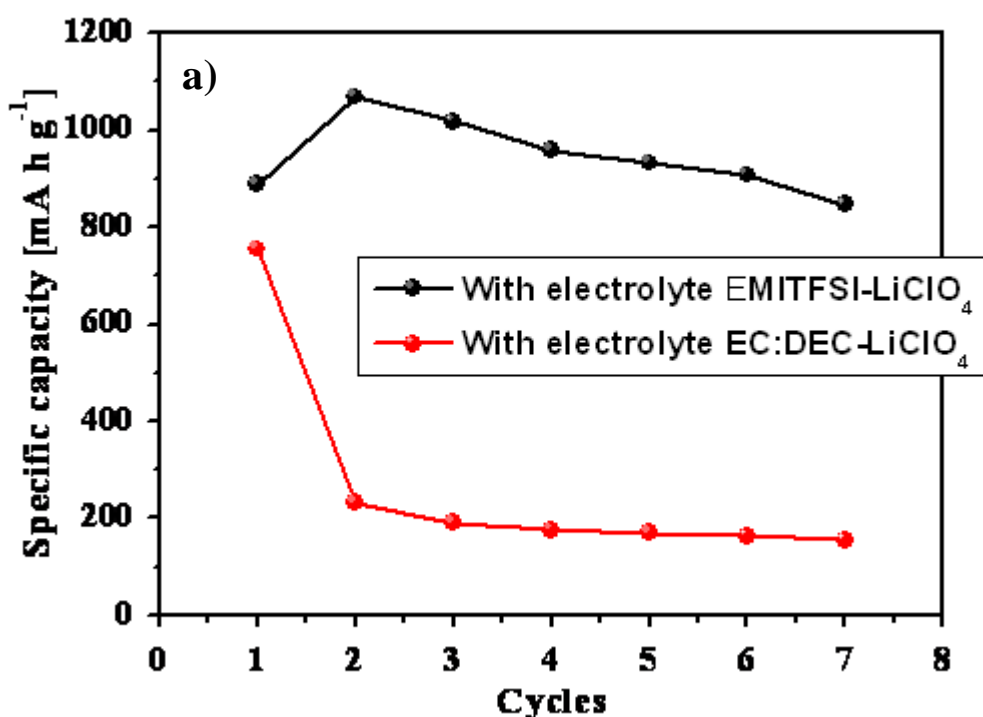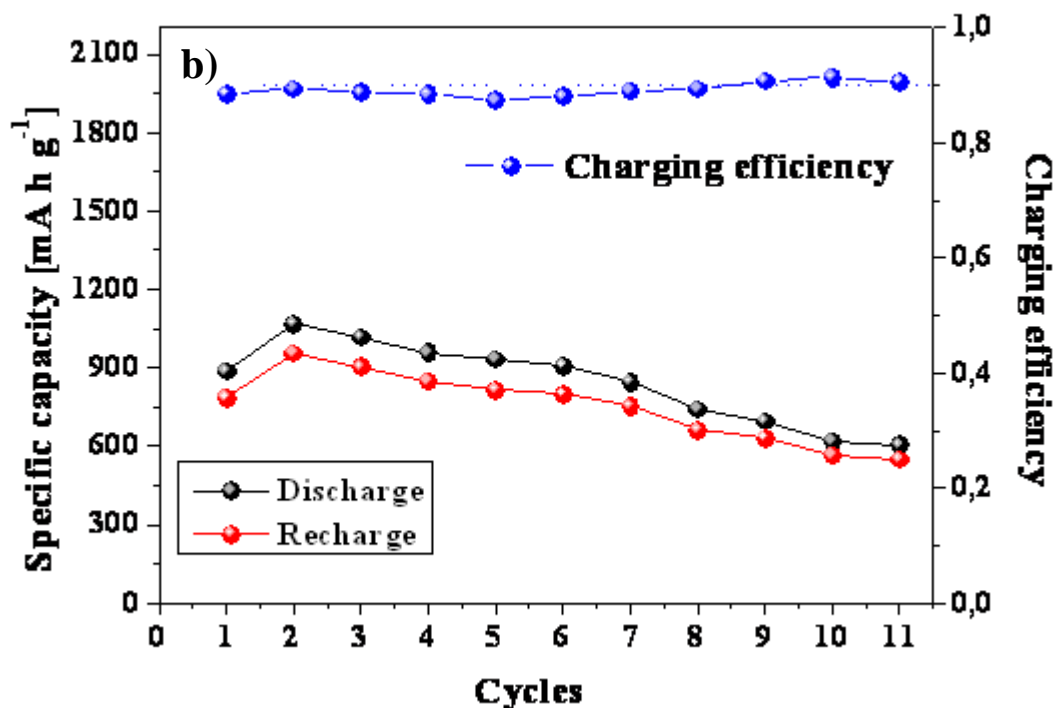
Figure 6. a) Specific capacity of the Li-O_2 cell with and without EMITFSI based electrolyte; b) The specific capacity (discharge/charge) vs. number of cycles of a cell based on EMITFSI-LiClO$_4$ with charging efficiency. The specific capacity calculated with respect to the total weight of carbon and α-MnO$_2$.

When 1.0 M LiClO$_4$ in 1:1 wt/wt ethylene carbonate (EC)-diethyl carbonate (DEC) electrolyte was used, the discharge capacity fell down to a very low value of 200 mAhg^{-1} immediately after the first cycle and the cell was almost dead even after 5 cycles. Indeed the cell with EMITFSI/LiClO$_4$ electrolyte maintained a high discharge capacity higher than 900 mAhg^{-1} during the first five cycles, and then slightly decreased during the subsequent cycles. This cell displayed a good cycling ability with a recharging efficiency of ~90% after 7 cycles (Fig.6a and b). The obtained specific capacity reported in this article was calculated with respect to the total weight of carbon and α-MnO$_2$.

Despite the possibility to reduce the Li$_2$O$_2$; Li-O$_2$ cells recharged with organic electrolytes involved not only in the reduction of lithium peroxide but also in the decomposition of the electrolyte (organic carbonates). The low capacity retention during cycling of Li-O$_2$ cells with alkyl carbonate electrolytes has also been reported by Freunberger *et al*., [21] and they explained the low performance of the cell to the repeated decomposition of the electrolyte on discharge followed by the oxidation of the decomposition products during cell re-charge. Both electrolytes evaporation and accumulation of Li carbonate, Li alkyl-carbonates, Li acetate and Li formate at the oxygen cathode could lead to a progressive electrolyte starvation, hence cycling cannot be prolonged anymore. Similar considerations were reported by Xu and Co-workers [47], who identified the consumption and decomposition of the organic carbonate solvent as the main reason for the poor cell performance and short cycle life. Although α-MnO$_2$ is responsible to catalyze the decomposition of organic solvent, the same reactions

occurred even in the absence of a catalyst during cycling of Li-O_2 cells [21], shed light on the role of working potential range for a complete cell, because the presence of oxygen can really alter the stability conditions of the electrolyte. The different cycling behaviours can be clearly seen if alkyl-carbonates are replaced by RTILs as the electrolyte. According to our experimental results, such differences can be related to the stabilization exerted by the RTIL: its low degradation as well as negligible evaporation during prolonged cycling which in turn assures the wetting of the separator and a deep reach of the electrolytes to the surface of the lithium peroxides, thus facilitating the ORR process.

3.3. Post mortem of the Li-O_2 cell
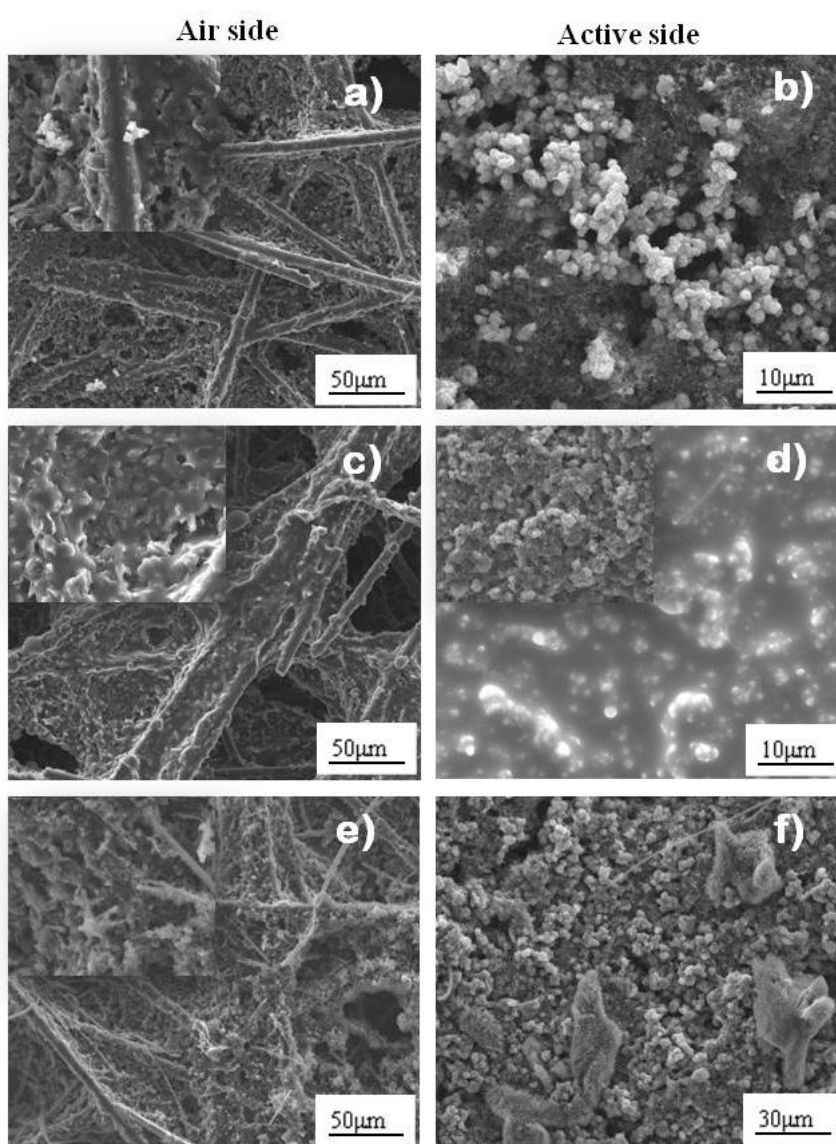
Figure 7. FESEM micrographs: morphologies of fresh air cathode in a cell exposed to air (air side) and exposed to electrolyte (active side) (a and b); tested cathode in RTIL electrolyte (c and d); tested cathode in organic electrolyte (e and f).

The FESEM examination of O_2-cathodes of two cells after cycling with different types of electrolytes is shown in Fig. 7. According to our experimental results, the considerable cyclability of the cells tested in EMITFSI-LiClO$_4$ electrolyte is due to the stabilization exerted by the electrolyte, lowering its degradation-evaporation during cycling. The active side of the oxygen cathode tested in RTIL was covered by a thin layer of electrolyte (Fig. 7d). After the electrolyte removal with acetone (Fig. 7d/inset), the tested electrode showed an unchanged porosity with respect to the pristine one (Fig. 7b). Fig. 7c showed that the air exposed side of the cathode, also maintained the porosity of the fresh one (Fig. 7a). The cathode which preserved plentiful electrolyte and well-maintained porous structure guaranteed high ionic conductivity as well as continuous and efficient O_2 diffusion, thus resulting in a significantly improved cycle capability in the Li-O_2 cell.

It is evident from Fig. 7(e and f) that the cathode tested with EC:DEC-LiClO$_4$ appears covered by a layer of evaporated electrolyte crystals even after very few cycles. The O_2 cathode as well as the separator of the cell containing the organic electrolyte was totally dry. This could be due to the evaporation of organic electrolyte solvent when the cell was purged with dry O_2 during testing. Similar results were also reported by Kuboki [29].

The sustainable catalytic activity of α-MnO$_2$ was attributed to its robust structure. The morphology and particle size of α-MnO$_2$ in the cathode were found to be unchanged after the first discharge/charge cycle at FESEM analysis. The α-MnO$_2$ was not covered by any insoluble intermediates and/or products after the first cycle. FESEM analysis of the crystal structure of α-MnO$_2$ (Fig.8) before and after the first discharge-recharge cycle confirmed that α-MnO$_2$ preserved its structure during cycling without any noticeable modifications hence assured a good cycle stability.
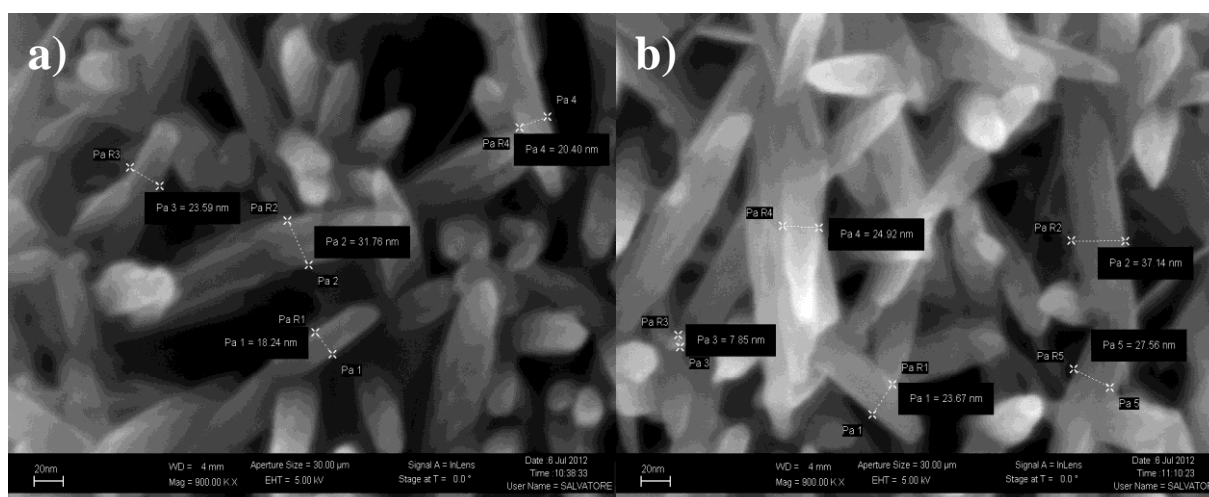
Figure 8. FESEM images of α-MnO$_2$: a) in the fresh electrode; b) after first cycle

4. CONCLUSION

A bimodal porous α-MnO$_2$ exhibiting a high BET specific surface area exceeding 156 m^{2}g^{-1} was easily synthesized by a simple and low cost procedure. The presence of α-MnO$_2$ in the oxygen cathode of a rechargeable Li-O_2 cell improved the discharge capacity as well as the cycle life of the system. In fact, an initial capacity of 900 mAhg^{-1} was obtained, which is higher than that obtained

when tested without the catalyst. The preliminary data suggest that ionic liquids are promising as safe, environmentally benign and durable electrolytes for rechargeable Li-O$_2$ cells. Additional experiments are necessary to define the kind of catalytic action exhibited by α-MnO$_2$ and also the type and composition of the RTIL-based electrolyte in order to optimize the stability in presence of both Li$^+$ ions and oxygen. Moreover, work is in progress to control both the particle and pore size of α-MnO$_2$ to improve its catalytic efficiency.

References

1. T. Ogasawara, A. Debart, M. Holzapfel, P. Novak and P.G. Bruce, *J. Am. Chem. Soc.* 128 (2006) 1390
2. Y. Lu, H. A. Gasteiger and Y. Shao-horn, *J. Am. Chem. Soc*. 133 (2011) 19048
3. P. G. Bruce, S. A. Freunberger, L. J. Hardwick and J.M. Tarascon, *Nat. Mater*. 11 (2012) 19
4. W. Xu, K. Xu, V. Viswanathan, S.A. Towne, J. S. Hardy, J. Xiao, Z. Nie, D. Hu, D. Wang and J. G. Zhang, *J. of Power Sources* 196 (2011) 9631
5. Y. C. Lu, H. A. Gasteiger, M. C. Parent, V. Chiloyan and Y. Shao-Horn, *Electrochem. Solid State Lett.* 13 (2010) A69
6. Y. C. Lu, Z. C. Xu, H. A. Gasteiger, S. Chen, K. Hamad-Schifferli and Y. Shao-Horn, *J. Am. Chem. Soc.* 132 (2010) 12170
7. D. Zhang , Z. H. Fu , Z. Wei, T. Huang and A. S. Yu, *J. Electrochem. Soc*. 157 (2010) A362
8. Z. H. Fu , X. J. Lin, T. Huang and A. S. Yu, *J. Solid State Electrochem.* 16 (2012) 1447
9. E. M. Benbow, S. P. Kelly, L. Zhao, J. W. Reutenauer and S. L. Suib, *J. Phys. Chem.* C 115 (2011) 22009
10. R. Black, S. H. Oh, J. H. Lee, T. Yim, B. Adams and L. F. Nazar, *J. Am. Chem. Soc*. 134 (2012) 2902
11. D. Capsoni, M. Bini, S. Ferrari, E. Quartarone and P. Mustarelli, *J. Power Sources* 220 (2012) 253
12. A. K. Thapa and T. Ishihara, *J. Power Sources* 196 (2011) 7016
13. H. Cheng and K. Scott, *J. of Power Sources* 195 (2010) 1370
14. H. Cheng and K. Scott, *Applied Catalysis B: Environmental* 108–109 (2011) 140
15. A. Débart, A. J. Paterson, J. Bao and P. G. Bruce, *Angew. Chem. Int. Ed*. 47 (2008) 4521
16. B. Li, G. Rong, Y. Xie, L. Huang and C. Feng. *Inorg. Chem. Aug*. 45 (2006) 6404
17. G. Q. Zhang, J. P. Zheng, R. Liang, C. Zhang, B. Wang, M. Au, M. Hendrickson and E. J. Plichta *J. Electrochem. Soc.* 158 (2011) A822
18. S. Freunberger, L. Hardwick, Z. Peng, V. Giordani, Y. Chen, P. Maire, P. Nova´k, J. Tarascon, and P. Bruce, Abstract 830, International Meeting on Lithium Batteries (IMLB), Montreal, 27 June to 2 July, 2010
19. V. Giordani, S. A. Freunberger, P. G. Bruce, J. M. Tarascon and D. Larcher, *Electrochem. Solid St*. 13 (2010) A180
20. J. H. Cheng, G. Shao, H. J. Yu and J. J. Xu, *J. Alloys and Compounds* 505 (2010) 163
21. S. A. Freunberger, Y. Chen, Z. Peng, J. M. Griffin, L. J. Harwick, F. Bardè, P. Novak and P. G. Bruce, *J. Am. Chem. Soc*., 133 (2011) 8040

22. W. Xu, V. V. Viswanathan, D. Wang, S. A. Towne, J. Xiao, Z. Nie, D. Hu and J. G. Zhang, *J. Power Sources* 196 (2011) 3894
23. H. G. Jung, J. Hassoun, J. B. Park, Y. K. Sun and B. Scrosati, *Nat. Chem.* 4 (2012) 579
24. W. Xu, J. Xiao, D. Wang, J. Zhang and J. G. Zhang, *Electrochem. Solid St*. 13 (2010) A48
25. Z. Peng, S. A. Freunberger, Y. Chen and P. G. Bruce, *Science* 337 (2012) 563
26. C. Gerbaldi, J. R. Nair, S. Ahmad, G. Meligrana, R. Bongiovanni, S. Bodoardo and N. Penazzi, *J. Power Sources,* 195 (2010) 1706
27. A. Fernicola, F. Croce, B. Scrosati, T. Watanabe and H. Ohno, *J. Power Sources* 174 (2007) 342
28. L. Cecchetto, M. Salomon, B. Scrosati and F. Croce, *J. Power Sources* 213 (2012) 233
29. T. Kuboki, T. Okuyama, T. Ohsaki and N. Takami, *J. of Power Sources* 146 (2005) 766
30. C. J. Allen, S. Mukerjee, E. J. Plichta, M. A. Hendrickson and K. M. Abraham, *J. Phys. Chem. Lett*. 2 (2011) 2420
31. S. D. Beattie , D. M. Manolescu and S. L. Blair , *J. Electrochem. Soc*. 156 (2009) A44
32. S. S. Zhang , D. Foster and J. Read , *J. Power Sources* 195 (2010) 1235
33. S. Oswald, D. Mikhailova, F. Scheiba, P. Reichel, A. Fiedler and H. Ehrenberg, *Anal. Bioanal. Chem* 400 (2011) 691
34. J. R. Nair, C. Gerbaldi, M. Destro, R. Bongiovanni and N. Penazzi, *React. Fun. Poly*. 71 (2011) 409
35. R. E. Williford and J. G. Zhang, *J. Power Sources* 194 (2009) 1164
36. Z. Li, Y. Ding, Y. Xiong, Q. Yang and Y. Xie, *Chem. Commun*. 7 (2005) 918
37. X. Wang, K. N. Bozhilov and P. Feng, *J. Am. Chem. Soc*. 129 (2007) 1690
38. B. Li, G. Rong, Y. Xie, L. Huang and C. Feng, *Inorg. Chem*. 45 (2006) 6404
39. L. G. Xue, H. Hao, Z. Wei, T. Huang and A. S. Yu, *J. Solid State Electrochem*. 15 (2011) 485
40. V. Subramanian, H. W. Zhu, R. Vajtai, P. M. Ajayan, and B. Q. Wei, *J. Phys. Chem.* B 109 (2005) 20207
41. G. Girishkumar, B. McCloskey, A. C. Luntz, S. Swanson and W. Wilcke, *J. Phys. Chem. Lett*. 1 (2010) 2193
42. Y. Shao, F. Ding, J. Xiao, J. Zhang, W. Xu, S. Park, J. G. Zhang, Y. Wang and J. Liu, Adv. Fun. Mat. (2012) DOI: 10.1002/adfm.201200688
43. C. S. Johnson, D. W. Dees, M. F. Mansuetto, M. M. Thackeray, D. R. Vissers, D. Argyriou, C. K. Loong and L. Christensen, *J. Power Sources* 68 (1997) 570
44. J. S. Lee, S. T. Kim, R. Cao, N. S. Choi, K. T. Lee and J. Cho, *Adv. Energy Mat.* 1 (2011) 34
45. A.Kraytsberg and Y. Ein-Eli, *J. Power Sources* 196 (2011) 886
46. J. Li, N. Wang, Y. Zhao, Y. Ding and L. Guan, *Electrochemistry Communications* 13 (2011) 698
47. W. Xu, K. Xu, V. V. Viswanathan, S. A. Towne, J. S. Hardy, J. Xiao, Z. Nie, D. Hu, D. Wang and J. G. Zhang, *J. Power Sources* 196 (2011) 9631